Morphology-controlled synthesis, growth mechanism, optical and microwave absorption properties of ZnO nanocombs

2008 J. Phys. D: Appl. Phys. 41 185405

(http://iopscience.iop.org/0022-3727/41/18/185405)

IOP PUBLISHING JOURNAL OF PHYSICS D: APPLIED PHYSICS

J. Phys. D: Appl. Phys. **41** (2008) 185405 (13pp) doi:10.1088/0022-3727/41/18/185405

Morphology-controlled synthesis, growth mechanism, optical and microwave absorption properties of ZnO nanocombs

R F Zhuo[1], H T Feng[1], Q Liang[1], J Z Liu[1], J T Chen[1], D Yan[1], J J Feng[1], H J Li[1], S Cheng[1], B S Geng[1], X Y Xu[1], J Wang[1], Z G Wu[1], P X Yan[1,2,4] and G H Yue[3]

[1] Department of Physics, Lanzhou University, Lanzhou 730000, People's Republic of China
[2] Key Laboratory of Solid Lubrication, Institute of Chemistry and Physics, Chinese Academy of Science, Lanzhou 730000, People's Republic of China
[3] Department of Materials Science and Engineering, Xiamen University, Xiamen 361005, People's Republic of China

E-mail: pxyan@lzu.edu.cn

Received 25 May 2008, in final form 7 July 2008
Published 28 August 2008
Online at stacks.iop.org/JPhysD/41/185405

Abstract

ZnO nanocombs and nanorods with different morphologies have been successfully synthesized through a simple metal vapour deposition route at 600–750 °C using pure zinc powder or zinc and graphite powders as source materials. The structures and morphologies of the products were characterized in detail by using x-ray diffraction, scanning electron microscopy, transmission electron microscopy and laser Raman spectrometer. The morphologies of the products can be easily controlled by tuning the following four factors: reaction temperature, the distance between the source and the substrates, the kinds of substrates and the kinds of precursors. Possible growth mechanisms for the formation of ZnO nanostructures with different morphologies are discussed. Photoluminescence studies show that there are sharp UV and broad defect-related green emissions for all products. Relative intensity of the UV to defect-related green emissions decreases from ZnO nanorods to nanocombs. Microwave absorption properties of these nanocombs are also investigated. The value of the minimum reflection loss is −12 dB at 11 GHz for the ZnO nanocomb composite with a thickness of 2.5 mm.

(Some figures in this article are in colour only in the electronic version)

1. Introduction

Zinc oxide, with a wide band gap of 3.37 eV and a large exciton binding energy of 60 meV at room temperature, is an important semiconducting material [1], which has four key properties. First, the wide band gap and the large exciton binding energy make ZnO suitable for short wavelength optoelectronic applications and ensure efficient excitonic emission at room temperature. ZnO is transparent to visible light and can be made into highly conductive materials by doping. Second, owing to its noncentral symmetry, ZnO is not only semiconducting but also piezoelectric and pyroelectric. It is a smart material and has versatile applications in the fields of piezoelectric nanogenerators [2], ultrasensitive nano-sized gas sensors [3], transducers and resonators [4]. Third, the element zinc is one of the most highly valuable elements for human beings. Its oxide, ZnO, is bio-safe and biocompatible, and it can be used for biomedical applications without coating [5]. Finally, ZnO nanostructures can be used as microwave absorbing materials motivated by their lightweight and semiconductive properties and also by the fact that their large-scale synthesis can be easily realized [6]. Since Yang and co-workers [7] reported on ZnO nanowire arrays in 2001, the synthesis and assembly of ZnO

[4] Author to whom any correspondence should be addressed.

nanostructures, such as nanowires, nanobelts and nanotubes, have been widely explored and many methods relying on vapour phase approaches and chemical solution process have been developed [1–26]. Some delicate hierarchical ZnO nanostructures with 2-, 4- and 6-fold symmetries were also obtained [8–11]. Wang and co-workers have successfully fabricated a variety of ZnO nanostructures by high-temperature ($\geqslant$950 °C) vapour transport and condensation (VTC) process using ZnO powder as the source material [12].

The structure of ZnO can be described as a number of alternating planes composed of tetrahedrally coordinated O^{2-} and Zn^{2+} ions stacked along the *c*-axis. The oppositely charged ions produce positively charged (0 0 0 1) Zn-polar and negatively charged (0 0 0 $\bar{1}$) O-polar surfaces, resulting in a normal dipole moment and spontaneous polarization along the *c*-axis [13]. Due to its hexagonal wurtzite structure, in which the three fastest growth directions, $\langle 0\,0\,0\,1\rangle$, $\langle 0\,1\,\bar{1}\,0\rangle$ and $\langle 2\,\bar{1}\,\bar{1}\,0\rangle$, and its polar crystal surfaces exist, ZnO exhibits a large family of nanostructures [12]. In addition to the conventional nanowire and nanobelt structures, a diverse group of novel ZnO nanostructures has been discovered recently, such as nanocages [14], nanorings [15], nanohelixes/nanosprings [16], nanobows [17], nanodiscs [18], nanotetrapods [19] and nanocombs [13, 19–26]. These novel nanostructures not only indicated that ZnO contains probably the richest family of nanostructures among all materials, in both structures and properties, but also provided valuable models in understanding crystal growth mechanisms in nanometre scale and exhibited high potential for fabricating novel nanoelectronic and optical devices with enhanced performance. Among all these different structures, ZnO comb-like structures are of interest for nanocantilever arrays [13], laser arrays [21], nanocomb biosensors [22] and gratings [23].

In this paper, we report a very simple metal vapour deposition (MVD) route to large-scale synthesis of ZnO nanocombs with quite complicated structures. By using metallic pure zinc powder or zinc and graphite powders as source materials, we can not only dramatically lower the growth temperature to 600 °C, but we can also easily control the morphologies of the obtained ZnO nanocombs by simply tuning the following four factors: reaction temperature, the distance between the source and the substrates, the kinds of substrates and the kinds of precursors. We suggest a growth model to explain the possible growth mechanism. The optical and microwave absorption properties of these nanocombs are also investigated at room temperature. Our results not only clearly support that the (0 0 0 1) Zn-polar surface is chemically active for inspiring self-catalysis, which leads to the formation of the comb structure [13], but also suggest that nanostructures of this type are ideal objects for the fabrication of nanoscale functional devices and may find applications in a variety of fields.

2. Experimental details

The ZnO nanocombs were synthesized via a simple MVD process in a quartz tube furnace system [27]. An illustration of the reaction system is shown in figure 1(*a*). The temperature

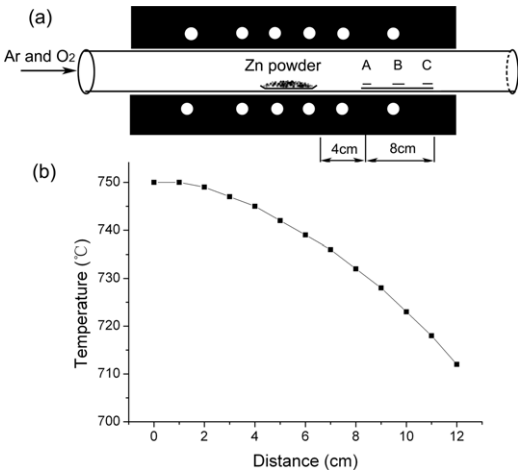

Figure 1. (*a*) Schematic illustration of the reaction system. (*b*) The temperature gradient of the furnace from the centre to the end of the quartz tube.

gradient was thus established from the centre to the end of the quartz tube (with an outer diameter of 42 mm, inner diameter of 35 mm and length of 800 mm), as shown in figure 1(*b*). In a typical process, zinc powder (purity of ~99.998%) was loaded in a ceramic boat. The boat was put in the centre of the furnace. Three pieces of substrate (named A, B and C) were placed 4–12 cm downstream of the zinc source, respectively. The (1 0 0)-oriented p-type silicon and anodic aluminium oxide (AAO) templates were used as the deposition substrates. After the quartz tube was evacuated by a mechanical rotary pump, the temperature of the furnace central region was raised to 600 °C–750 °C with a heating rate of 30 °C min^{-1}. High-purity Ar and O_2 gases, whose flow rates were separately controlled by two flowmeters at Ar 140 sccm and O_2 10 sccm, were introduced into the inner quartz tube. The temperature was maintained for 15–20 min. Afterwards, the furnace was cooled down to room temperature naturally.

The as-synthesized ZnO nanostructures were studied by x-ray diffraction (XRD) on a X'Pert PRO PHILIPS diffractometer using Cu Kα irradiation (λ = 1.540 56 Å), field-emission scanning electron microscopy (FE-SEM, Hitachi S-4800 and JEOL JSM6701-F) equipped with energy dispersed x-ray spectroscopy (EDS), TEM and SAED was carried out on a Hitachi H-600 transmission electron microscope operated at 100 kV and HRTEM was carried out on a TECNAI F30 high-resolution transmission electron microscope. A fluorescence spectrophotometer (FLS920T) equipped with a xenon lamp was used for photoluminescence (PL) spectroscopy and the PL spectra were obtained at room temperature under an ambient atmosphere. Raman spectra were recorded at room temperature with a YVON HR800UV Laser Raman spectrometer. The composite samples used for microwave absorption measurement were prepared by mixing the ZnO nanocombs/nanorods with paraffin wax with 50 vol% of the ZnO nanocombs/nanorods. The mixtures were then pressed into toroidal shaped samples (ϕ_{out} : 7.00 mm, ϕ_{in} : 3.04 mm). The complex permittivity and permeability of the mixtures in the 0.1–18 GHz frequency range were

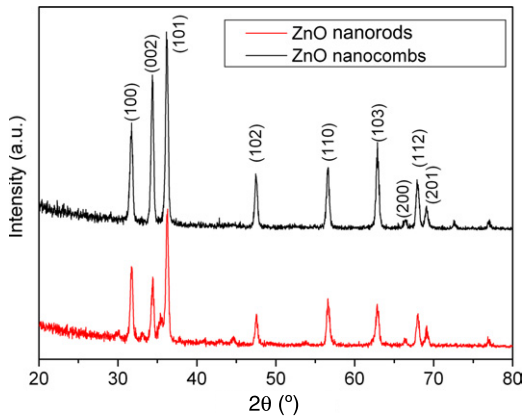

Figure 2. Typical XRD patterns of ZnO nanocombs and nanorods.

measured by using an Agilent E8363B vector network analyzer [28].

3. Results and discussion

3.1. Structural characterization and analysis

Figure 2 shows the XRD patterns of both ZnO nanocombs and nanorods. All the strong peaks in these patterns can be well indexed to hexagonal wurtzite ZnO ($a = 3.253$ Å, $c = 5.209$ Å, JCPDS file No.80-0075).

The Raman spectra of the ZnO nanostructures excited by laser lines 532 nm and 325 nm are illustrated in figures 3(a) and (b), respectively. According to the literature values, all the observed spectroscopic peaks listed in figure 3(a) can be assigned to a wurzite ZnO structure [29, 30]. Among these Raman peaks, the E_2 mode centred at 437 cm^{-1} has a stronger intensity and narrower line-width, which indicates that the as-grown products are composed of ZnO with a hexagonal wurtzite structure and good crystal quality. It is noted that the remarkable feature for $\lambda = 325$ nm excitation is dominated by the 1LO and multi-LO modes in the spectra which can be seen clearly in figure 3(b). This apparently exhibits the resonant Raman scattering (RRS) characteristic for hexagonal crystals [30]. Multi-LO phonon RRS has been reported for ZnO compounds, including films, nanostructures and single crystals [31].

3.1.1. ZnO nanocombs synthesized on silicon substrates at different temperatures. Figure 4 shows the SEM images of the ZnO nanostructures synthesized at 600 °C (temperature of the centre region of the furnace) on silicon substrates. Figures 4(a) and (b) show the products obtained from the substrate placed at A (about 3–4 cm downstream of the source). ZnO nanorods and some fragmentary nanocombs can be seen on a large scale. Figures 4(c) and (d) show the products obtained from the substrate placed at B (about 7–8 cm downstream of the source). It shows almost the same morphology as in place A. But from the images shown in figures 4(e) and (f) which were taken from the substrate placed at C (about 11–12 cm downstream of the source), it can be seen that large-scale, vertically aligned ZnO nanorods

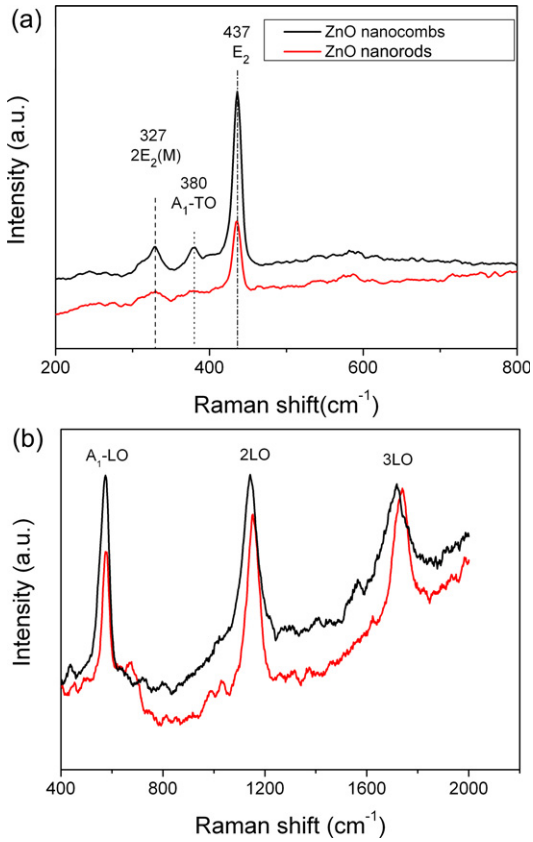

Figure 3. Typical Raman spectra of the ZnO nanostructures excited by laser lines: (a) 532 nm and (b) 325 nm.

have been uniformly grown on the silicon substrate. All the images indicate that the diameters of the nanorods are no longer uniform along their length, but gradually increase from the base to the top and end with a hexagonal cap, composed of nanocones. The diameters of the nanocones range from about 80 nm at the base to 300 nm at the top, and the lengths are about 1 μm.

Figure 5 shows the SEM images of the ZnO nanostructures synthesized at 650 °C on silicon substrates. Figure 5(a) shows that large-scale and high density ZnO nanotetrapods have been synthesized on the silicon substrate which was placed at A. From the inset it can be seen that the structures are of tetrahedral shape with four legs; the length of the legs is about 2 μm and each leg is a regular-shaped hexagonal cone arm which does not have a uniform diameter along its axes, but becomes thicker towards the tip and forms a hexagonal-shaped cap. Figure 5(b) shows the SEM images of the products obtained at place B. It is clearly seen that nanocombs blending with nanotetrapods have been synthesized. It can be noted that the nanotetrapods presented here are actually tripod-like arms at the end of nanowires; the base nanowires are several micrometres in length and tens of nanometres in diameter. Figure 5(c) shows the SEM images of the products obtained at place C; vertically aligned ZnO nanocones have been grown on the silicon substrate. The nanocones presented in figure 5 are somewhat different from those shown in figure 4; the hexagonal caps are flat and have no local contraction.

The SEM images of the product obtained at 700 °C on silicon substrates are shown in figure 6. Figures 6(a) and

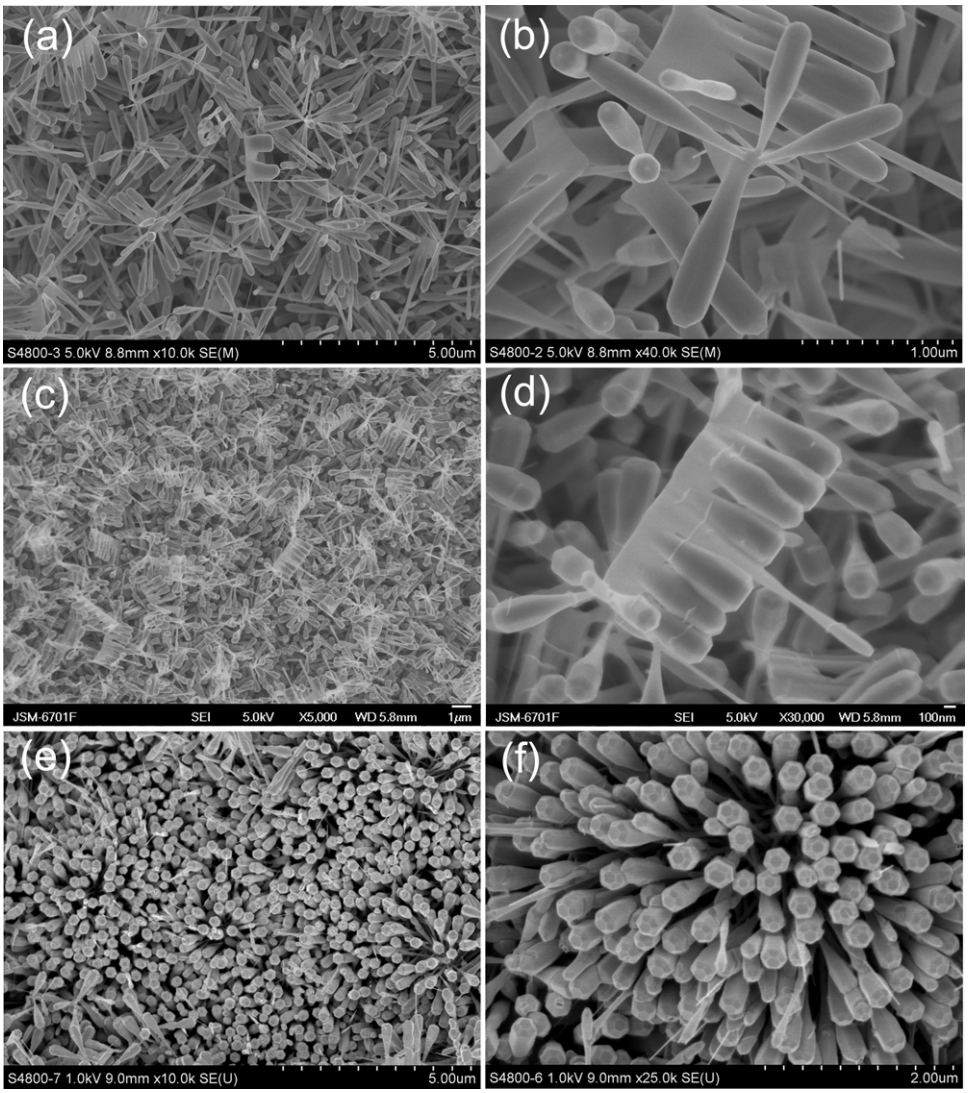

Figure 4. SEM images of the ZnO nanostructures synthesized at 600 °C on the silicon substrate: (*a*)–(*b*) placed at A, (*c*)–(*d*) placed at B and (*e*)–(*f*) placed at C.

(*b*) show the SEM images of the products obtained at place A. It can be seen that ZnO nanocombs and hierarchical nanostructures have been synthesized, and all the branches have very sharp tips. Figures 6(*c*) and (*d*) show the SEM images of the products obtained at place B; a number of intact ZnO nanocombs have been grown on the silicon substrate. The length of the branches is about 2 μm and each branch is an acicula-shaped cantilever which does not have a uniform diameter along its axes, but becomes thinner towards the tip and finally forms a very sharp and long tip. The diameters of branches range from about 200 nm at the base to 20 nm at the tip. Figures 6(*e*) and (*f*) show the SEM images of products obtained at place C; high density ZnO nano-aciculae have been grown on the silicon substrate.

Figure 7 shows the SEM images of the ZnO nanostructures synthesized at 750 °C on silicon substrates. Figures 7(*a*) and (*b*) show the SEM images of the products obtained at place A, and figures 7(*c*) and (*d*) show the SEM images of the products obtained at place B. They possess almost the same morphology. Both of them show that a number of ZnO nanocombs have been fabricated, but nanocombs at place B have a relative higher structural integrity than A. All the branches of combs are nanorods with a length of 5 μm and a uniform diameter of 50 nm. Figures 7(*e*) and (*f*) show the SEM images of the products obtained at place C. It can be seen that high density nanorods blending with a small quantity of nanocombs have been synthesized. The ZnO nanorods look like geminate chopsticks.

Further structural characterization of the ZnO nanocombs and nanorods synthesized on silicon substrates was performed by TEM and HRTEM. Figure 8(*a*) shows a typical TEM image of the ZnO nanocombs with hexagonal-shaped nanocone branches, and the inset shows the corresponding SAED of the circle marked area of the TEM image, which indicates that the growth direction of ZnO hexagonal-shaped nanocone branches is along [0 0 0 1] and the growth direction of the stem is along [0 1 $\bar{1}$ 0]. Figure 8(*b*) shows a typical TEM image of a single nanocone. The corresponding SAED pattern is shown in the inset; the single-crystal nature of ZnO hexagonal-shaped nanocones grown along the [0 0 0 2]

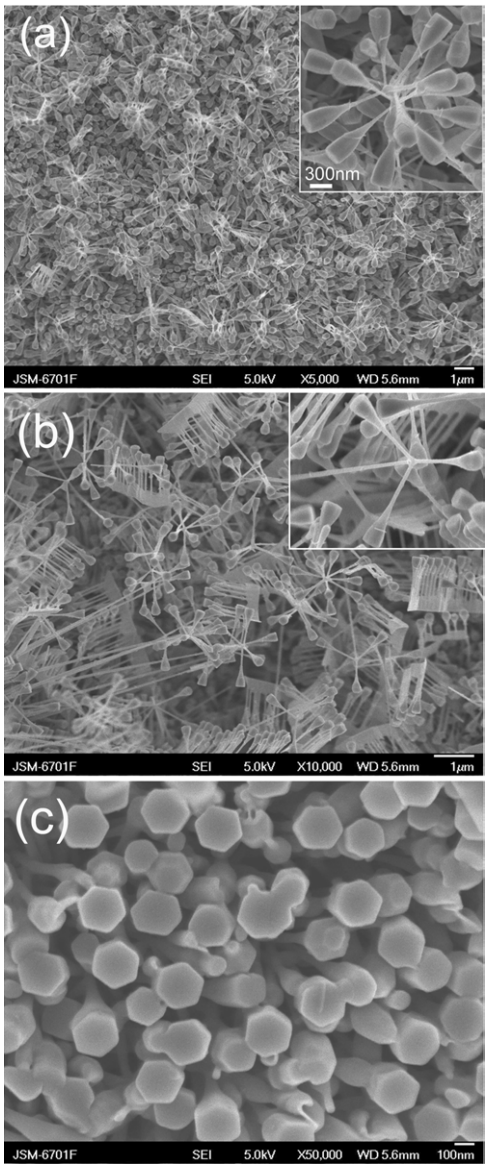

Figure 5. SEM images of the ZnO nanostructures synthesized at 650 °C on the silicon substrate: (*a*) placed at A, (*b*) placed at B and (*c*) placed at C.

direction can be seen. Figures 8(*c*) and (*d*) display TEM images of another two types of ZnO nanocombs. Figure 8(*e*) shows the high-resolution TEM image of the selected area in figure 8(*d*); crystal planes aligned perpendicular to the growth direction are clearly visible. The measured inter-plane spacing (0.52 nm) matches well with the literature value for the (0 0 0 2) plane in wurtzite ZnO (lattice parameter = 0.5196 nm), unambiguously reinforcing the conclusion that the ZnO branches grow along the [0 0 0 1] direction. HRTEM as well as SAED analysis confirms that the growth front of the ZnO nanocomb branches is along the *c*-axis, with side surfaces $\pm(0\,1\,\bar{1}\,0)$, and top/bottom surfaces $\pm(2\,\bar{1}\,\bar{1}\,0)$.

3.1.2. ZnO nanocombs synthesized on AAO template substrates with different precursors. In order to study the influence of substrates on the growth of ZnO nanocombs, different substrates were used. Figure 9 shows the SEM and TEM images of ZnO nanocombs synthesized by vaporizing pure zinc powder at 680 °C on the AAO template substrates placed at A. Figures 9(*a*) and (*b*) show that high density ultra-long and fine-orderly ZnO nanocombs have been grown on the surface of the AAO substrates. The inset in figure 9(*b*) shows that the stem of the ZnO nanocomb is an ultra-wide ZnO nanobelt and the branches are acicula-shaped ZnO nanorods. Figure 9(*c*) shows a representative SEM image of double-side toothed ZnO nanocombs. In figure 9(*d*), feather-like comb structures are shown, which have similar structures as the one shown in figure 9(*c*) except that the growth time is longer at 30 min. Figure 9(*e*) shows the TEM image of the ZnO nanocombs as shown in figure 9(*c*). Figure 9(*f*) shows the TEM image of the ZnO nanocombs as shown in figure 9(*d*); the symmetric nanocomb has two-sided teeth which are at an angle of about 110°. Figure 9(*g*) shows the TEM image of the as-grown single-sided ZnO combs. The corresponding SAED in figure 9(*h*) indicates that the growth direction of the ZnO nanocomb branches is along the [0 0 0 1] direction, with side surfaces $\pm(0\,1\,\bar{1}\,0)$ and top/bottom surfaces $\pm(2\,\bar{1}\,\bar{1}\,0)$.

All the above products use pure zinc powder as the Zn source for assembling ZnO nanocombs. Here we use zinc and graphite powders as the reaction Zn source. Figure 10 shows the SEM images of ZnO nanocombs synthesized by using zinc and graphite powders (1 : 1 wt%) as precursors at 700 °C on the AAO template substrates placed at A. Figures 10(*a*) and (*b*) show typical SEM images of the products grown for 15 min with different magnifications. The whole lengths of the combs are about 30–50 μm, and the perpendicular branches are a cuboid nanorod array. Figures 10(*c*) and (*d*) show typical SEM images of the products grown for 30 min with different magnifications. The SEM image in figure 10(*c*) gives a general overview of the ZnO nanocombs. The insets clearly show the typical rhombic or rectangular cross-section feature of the nanorods with widths in the 200–500 nm range.

3.2. Growth mechanism of ZnO nanocombs

The above analysis shows that different reaction temperatures and substrate places result in the formation of ZnO nanostructures with different morphologies. Further experiments show that the morphology of the final product in the thermal-evaporation process is mainly influenced by the following four factors.

i) Reaction temperature. We have shown that ZnO nanocombs synthesized at 600 °C–750 °C have distinct dissimilarities. Studies from SEM and TEM procedures show that the ZnO nanostructures formed in the present process are of very complex structures under different source temperatures. The branches of the ZnO combs and the ZnO nanorods change from cone-shaped to acicula-shaped nanorods. The possible mechanism is as follows. In this work, no metal catalyst was used, so the growth mechanism can be deduced to be the VS process. First, Zn is evaporated and oxidized by the oxygen in the reaction system to form ZnO_x gases. The newly formed ZnO_x gases are transported by Ar gas and deposited on the silicon substrate downstream to nucleate at an early stage. Second, further evaporation, oxidization

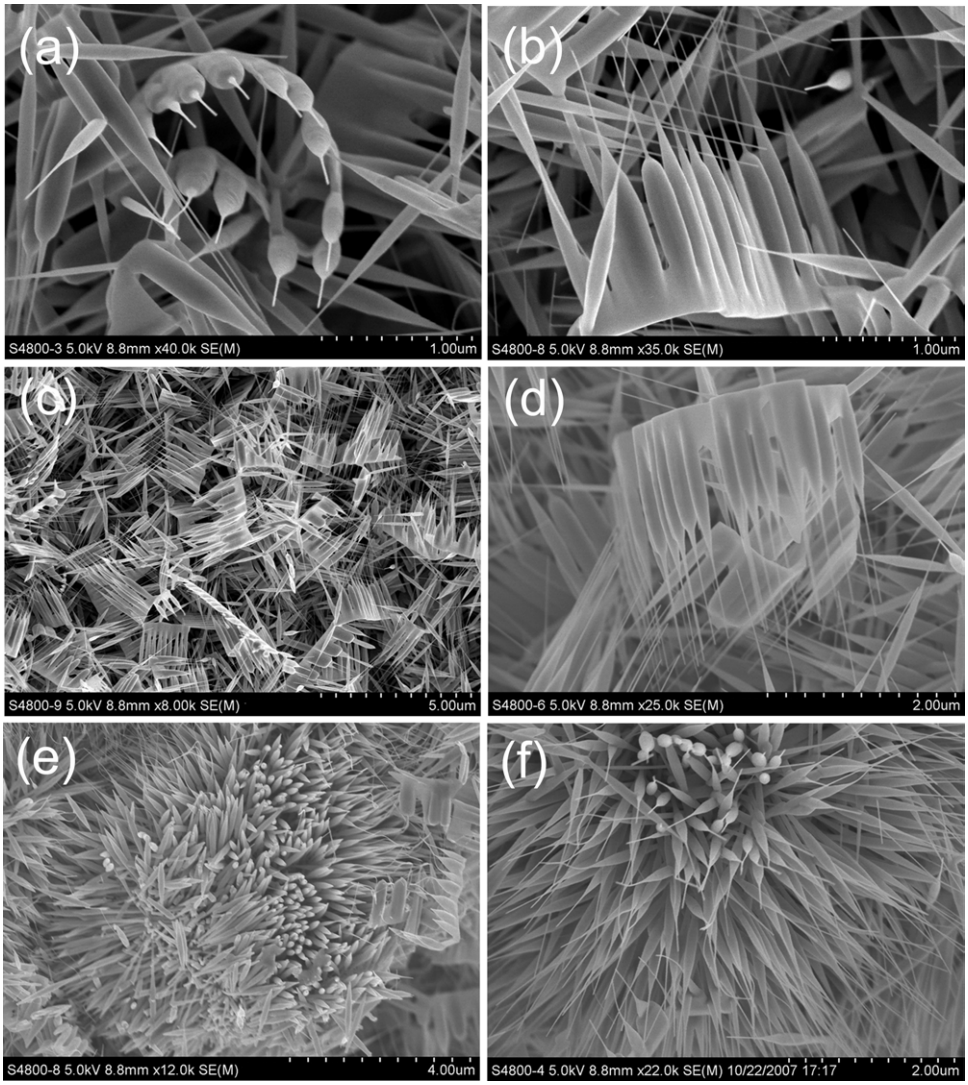

Figure 6. SEM images of the ZnO nanostructures synthesized at 700 °C on the silicon substrate: (*a*)–(*b*) placed at A, (*c*)–(*d*) placed at B and (*e*)–(*f*) placed at C.

and nucleation cause homogeneous epitaxial growth of ZnO nanostructures [32]. With the increase in temperature, the concentration of vaporized Zn gases increases considerably. It is well known that the concentration of Zn gases has a significant influence on the morphologies of the ZnO products. The incoming ZnO_x vapour is deposited and different ZnO nanostructures are formed due to the different deposited ratios [32]. We speculate that the differences in the branches of ZnO nanocombs and nanorods with increasing source temperature may be as follows: at a lower temperature, the Zn and ZnO_x vapours are generated slowly and the process of ZnO crystallization is also relatively slow, so the ZnO_x vapours formed a small diameter bottom. By prolonging the reaction, more ZnO_x vapours are generated and result in the formation of a cone-shaped shaft and finally a hexagonal flat cap is formed because the ZnO_x vapours are abundant and the cap of the nanocone takes a longer time to absorb the ZnO_x vapour than the bottom. At a higher temperature, the Zn and ZnO_x vapours are generated fast and they keep a steady rate at the beginning of the reaction so that a large diameter shaft was formed first. By prolonging the reaction, ZnO_x vapour is exhausted and few ZnO_x vapours deposit on the shaft, so an acicula-shaped nanorod with a small diameter tip is formed [32].

ii) The distance between the source and the substrates. We have discussed the products deposited on the silicon substrate placed at A, B and C. It can be found that ZnO nanocombs were deposited on the silicon substrates placed at A and B; when the distance increased, ZnO nanorods were synthesized on the substrates placed at C. In our experiment, the growth process may be as follows. As for the comb-like ZnO nanostructures grown on the substrate which was placed at A and B, in the first step, the fast growth rate is along the $[0\,1\,\bar{1}\,0]$ direction. In the subsequent second step, oxygen and zinc partial pressures were influenced by increasing the gas flux rate. This change in growth kinetics leads to the fast growth direction shifting to the $[0\,0\,0\,1]$ direction [24]. From the thermodynamic point of view, the $\pm(2\,\bar{1}\,\bar{1}\,0)$ planes act as relatively low energy surfaces in the reaction conditions of both steps and finally survive as the top/bottom surface in the belts and the branches. As for the ZnO nanorods grown on the substrates placed at C, the condition of the growth system does not change obviously. The pressure of zinc and oxygen is diluted all the

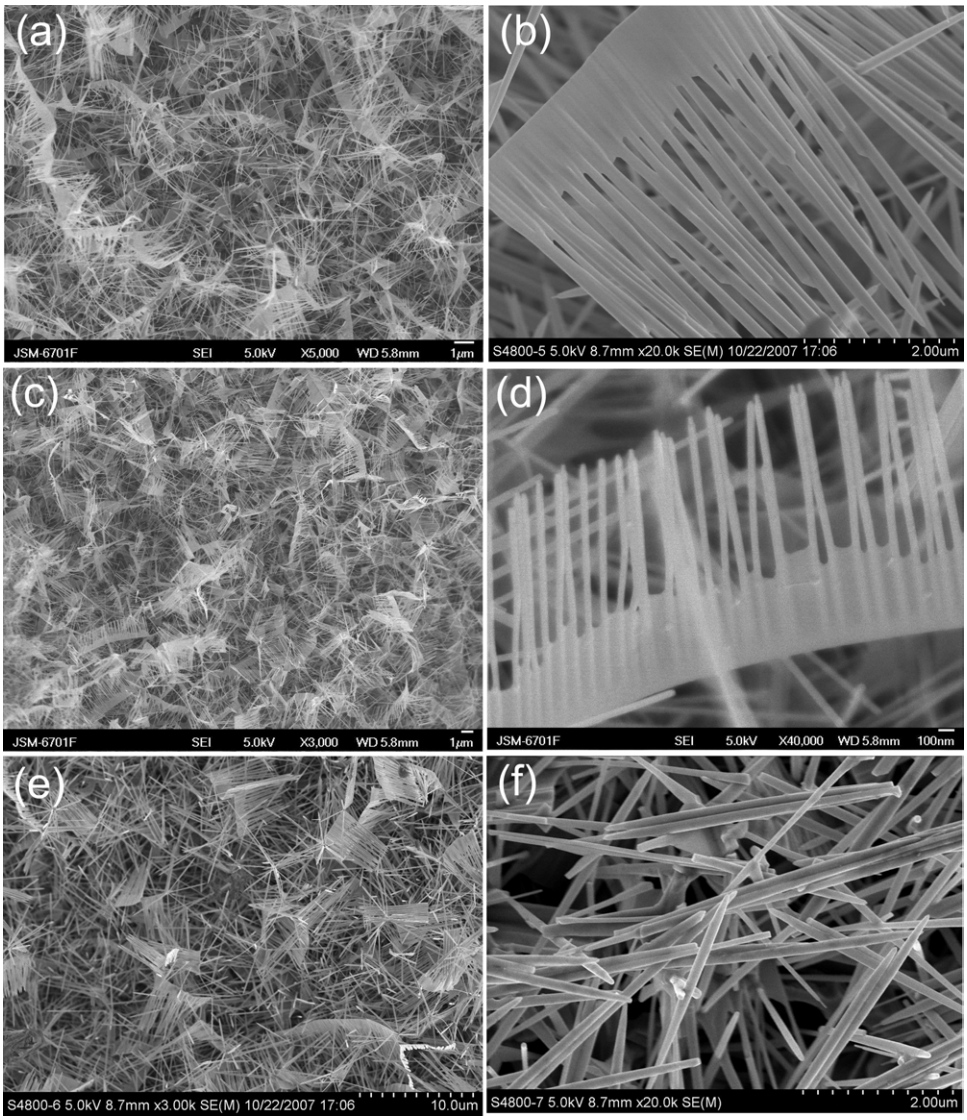

Figure 7. SEM images of the ZnO nanostructures synthesized at 750 °C on the silicon substrate: (*a*)–(*b*) placed at A, (*c*)–(*d*) placed at B and (*e*)–(*f*) placed at C.

time, so the nanostructures grow along the [0 0 0 1] direction and form nanorod arrays from the beginning to the end of the reaction. From the crystallography point of view, Zn supersaturation near the source (places A and B) is higher than far from the source (place C). Many researchers reported that low supersaturation benefits the growth of one-dimensional nanostructures [33]. In the growth of nanowires, the relatively lower supersaturation is probably critical for one-dimensional growth, which should be lower than that required for euhedral crystal growth, otherwise two- or three-dimensional growth will occur [34].

iii) Substrates. ZnO nanocombs synthesized on silicon substrates and AAO templates have distinct differences. ZnO nanocombs synthesized on smooth and polished silicon substrates are asymmetric one-sided combs (figures 4–8). On the rough and porous AAO templates, the ZnO nanocombs are asymmetric combs blending with double-sided combs (figure 9) and cuboid combs (figure 10). Since all the other conditions are the same, this indicates that the substrate significantly affects the growth of ZnO nanostructures. The different structures observed on AAO templates can be attributed to the large number of possible nucleation sites. The differences in the available nucleation sites and Zn diffusion rates on different substrates likely affect the subsequent nucleation and growth [20]. The formation of the double-sided nanocombs in figure 9 can be explained by the octahedral multiply twinned nucleus that is responsible for the formation of the tetrapod [25]. The central octahedral nucleus is composed of eight tetrahedral crystals which include four (0 0 0 1) planes and four (0 0 0 $\bar{1}$) planes all together, and they are of tetrahedral symmetry, respectively. If the nucleus contains only four tetrahedral units, in the shape of a half-octahedron, there are only two Zn-polar (0 0 0 1) planes; the growth of nanowires from the (0 0 0 1) planes leads to the formation of the structures presented in figures 9(*c*)–(*f*), with the teeth on both sides at an angle of 110° [25]. Such a structure has also been found for ZnS [35]. However, exactly how the octahedral multiply twinned nucleus nucleates is still unknown.

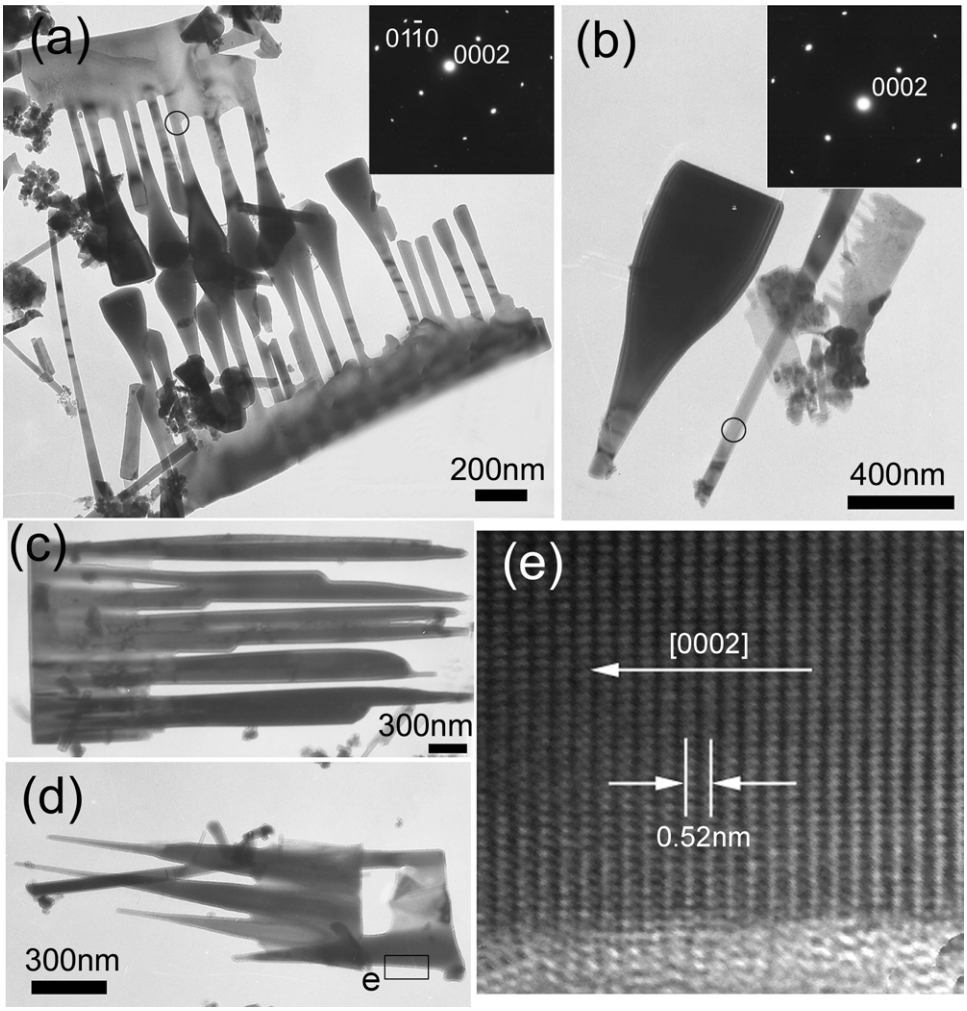

Figure 8. (*a*) A typical TEM image of the ZnO nanocombs with hexagonal-shaped nanocone branches, and the inset shows the corresponding SAED of the circle marked area. (*b*) A typical TEM image of a single nanocone; the inset shows the corresponding SAED pattern. (*c*)–(*d*) Typical TEM images of another two types of ZnO nanocombs. (*e*) The high-resolution TEM image of the selected area in (*d*).

iv) Precursors. The ZnO nanocombs synthesized on the AAO template using zinc and graphite powders (1 : 1 wt%) as precursors are very different from the ZnO nanocombs using pure zinc powder as the Zn source. Figure 10 shows the unique ZnO nanocombs with cuboid nanobranches. Here, we propose a possible growth mechanism for this unique comb-like structure. In the initial stage, the comb ribbon forms and grows along the [0 1 $\bar{1}$ 0] direction (figure 11(*a*)). Although some researchers reported that the impurity incorporation is substantially higher on the O-polar surface [36], that the Zn-polar surface is chemically active for inspiring self-catalysis and the (0 0 0 $\bar{1}$) O-polar surface is inert, has also been proven by many groups [13, 19–26]. Thus, the nuclei of the new ZnO branches form only on the (0 0 0 1) Zn-polar surface of the comb ribbon (figure 11(*b*)). And the [0 0 0 1] direction becomes the fastest growth direction for branching nanorods. As the branching nanorods grow, the ribbon stems continue to become wider and thicker with a lower growth velocity because of the relatively slower velocity along [2 $\bar{1}$ $\bar{1}$ 0] compared with the [0 0 0 1] direction for branching rods (figure 11(*c*)) [26]. This growth process is similar to that of the ordinary comb-like structures, if anything, it is the rate of release of Zn that is due to different precursors. The rate of release of Zn is relatively slow when using zinc and graphite powders (1 : 1 wt%) as precursors, and thus, the difference in the growth velocity along [0 0 0 1] and [0 1 $\bar{1}$ 0] is not so large accordingly. The crystal facet with the faster growth velocity disappears more easily and the facet with the slower growth velocity is prone to remain. Thus, the combination growth of the three directions can form short and cuboid branches (figures 11(*d*) and (*e*)), rather than form ordinary thin and rod-like branches (as shown in figures 4–9). However, further work is needed to make the exact mechanism clear.

3.3. PL and microwave absorption properties of ZnO nanocombs

3.3.1. PL property. Figure 12(*a*) shows the PL spectra of the as-grown ZnO nanocombs and nanorods, which are excited with a laser of 325 nm at room temperature. The PL spectra mainly include two parts: a sharp UV emission band centred at about 381 nm and a broad green emission band

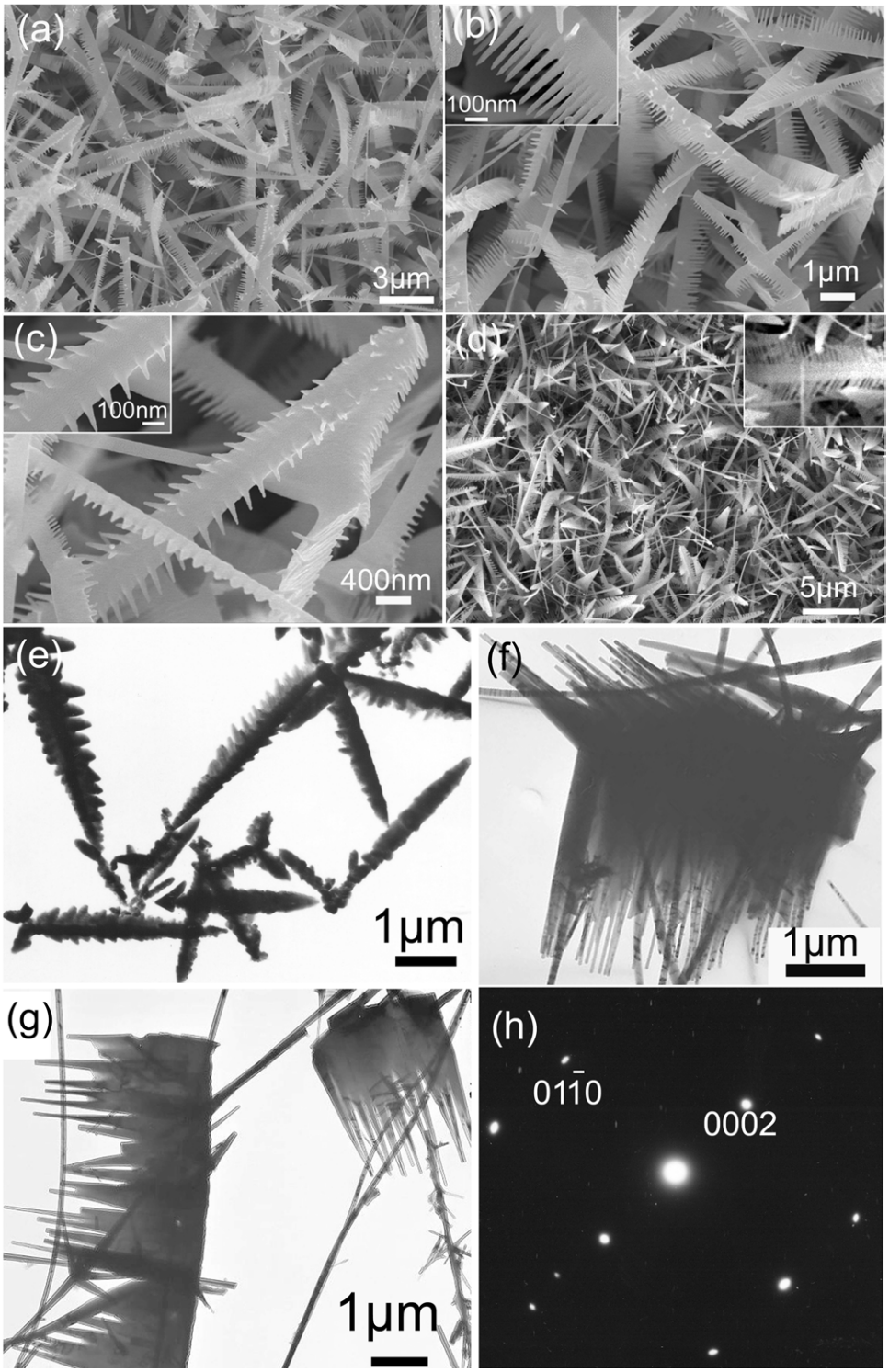

Figure 9. Typical SEM and TEM images of ZnO nanocombs synthesized by vaporizing pure zinc powder at 680 °C on AAO template substrates placed at A. (*a*)–(*b*) Typical SEM images of ZnO nanocombs in different magnifications. (*c*) A representative SEM image of double-side teeth ZnO nanocombs. (*d*) SEM images of feather-like ZnO nanocombs. (*e*)–(*g*) Typical TEM images of ZnO nanocombs. (*h*) The corresponding SAED patterns of (*g*).

at around 510 nm. The relative intensity ratio of the green-light emission to UV emission increases from nanorods to nanocombs. The UV emission is due to the recombination of free excitons in relation to the band gap, and the green-light emission originates from the deep level emission [37,38]. The origin of the green emission is somewhat controversial though there have been many reports on this emission. The commonly accepted explanation is that the green emission is due to a transition between a singly ionized oxygen vacancy and a photoexcited hole [38]. Other mechanisms, such as donor–acceptor complexes, antisite oxygen, Zn vacancy, were also proposed [37,38]. In our work, energy-dispersed spectroscopy

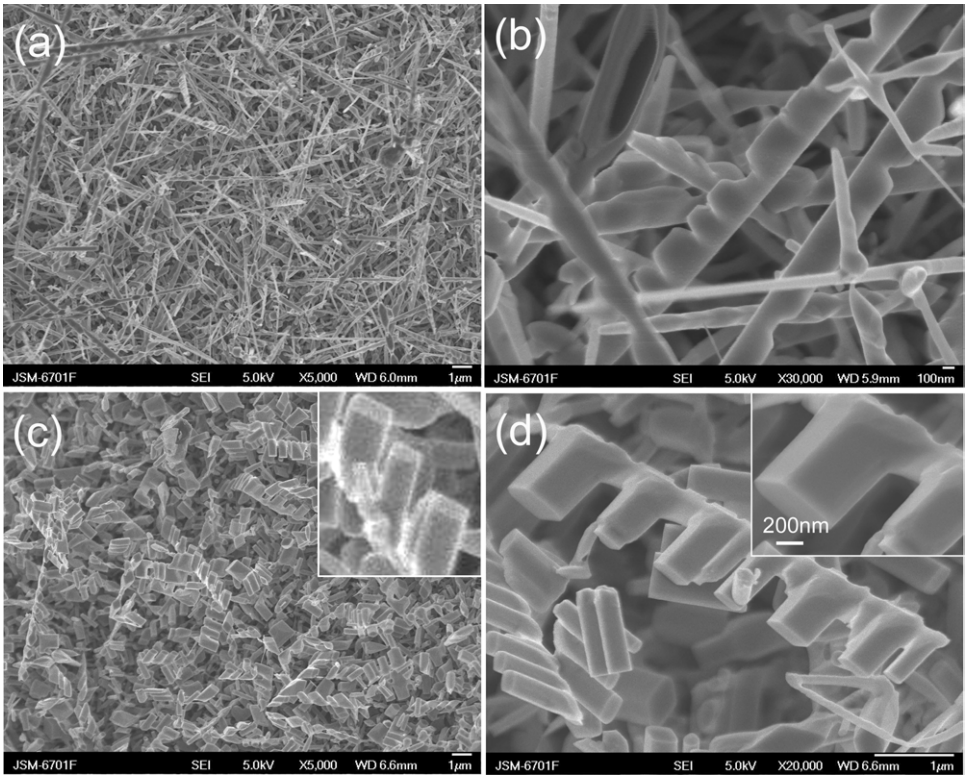

Figure 10. Typical SEM images of the unique ZnO nanocombs with cuboid nanobranches synthesized by vaporizing zinc and graphite powders at 700 °C on AAO template substrates placed at A. (*a*)–(*b*) ZnO nanocombs grown for 15 min, (*c*)–(*d*) grown for 30 min.

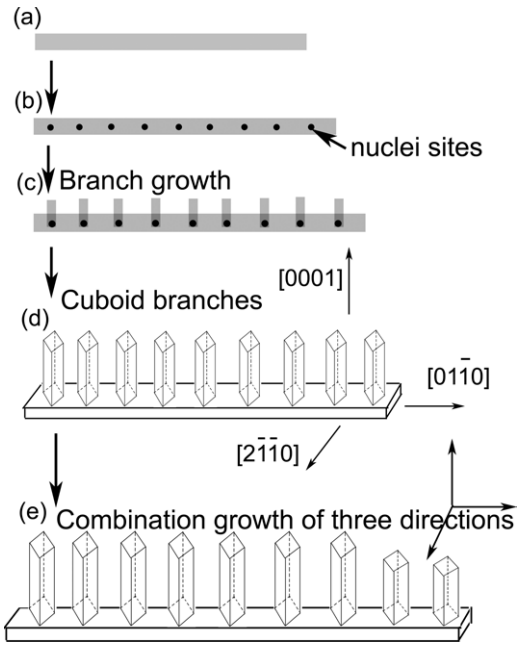

Figure 11. Schematic illustration of the proposed growth mechanism of ZnO comb-like structures with cuboid nanobranches. (*a*) Stem forming in the initial stage. (*b*) ZnO nuclei forming on the (0 0 0 1) surface of the comb stem. (*c*) Branching rods growing along the [0 0 0 1] direction. (*d*) Growing along three directions forming a rectangular cross-section. (*e*) A trapezium comb-like structure with a triangular profile forming.

(EDS) shows that the element ratio of Zn : O is 1 : 1.39 for the ZnO nanocombs (as shown in figure 12(*b*)) , which indicates that the ZnO nanocombs are O-rich. Therefore, the main point defects should be the Zn vacancy (V_{Zn}) defects [37, 38]. Associated with the EDS results, it is reasonable to conclude that in our ZnO nanocombs Zn vacancies (V_{Zn}) should be the most possible origin of the green emission. In addition, ZnO nanocombs possess more complicated structures and interfaces than nanorods. Thus, the point defect density of the ZnO nanostructures and the intensity of the green-light emission increase when the morphology changes from nanorods to hierarchical nanocombs.

3.3.2. Microwave absorption properties of ZnO nanocombs/paraffin composite. Recently, nanostructured materials have attracted considerable interest as microwave radiation absorbing and shielding materials in the GHz frequency range due to their unique chemical and physical properties [6]. Considering the light weight and semiconductive properties of the ZnO nanocombs and that large-scale synthesis of the ZnO nanocombs can be easily realized, they may have potential applications in electromagnetic interference shielding materials. Thus, it is necessary to study the novel properties of this unique nanostructure.

Figure 13 shows the complex permittivity ($\varepsilon_r = \varepsilon'_r - j\varepsilon''_r$) of the ZnO nanorod composite with 50% ZnO nanorods and the ZnO nanocomb composite with 50 vol% ZnO nanocombs. Figure 13(*a*) shows the real permittivity (ε'_r) of the two composites. The ε'_r values of the ZnO nanorod composite decline with increasing frequency from 10 to 5 in 0.1–18 GHz, and the ε'_r values of the ZnO nanocomb composite decline with increasing frequency from 12 to 8 in 0.1–18 GHz and exhibit a peak at 13–17 GHz. Figure 13(*b*) shows the imaginary permittivity (ε''_r) of the two composites. The ε''_r values show a different variation; for the ZnO nanorod composite, the ε''_r

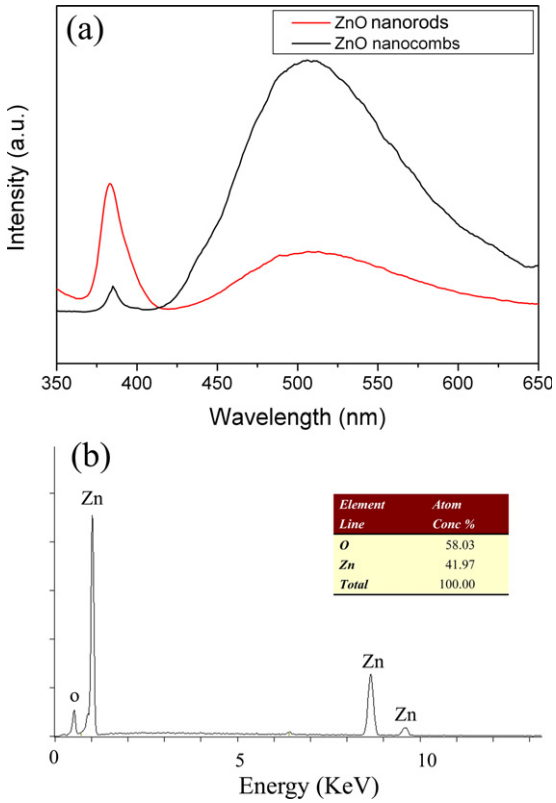

Figure 12. (*a*) Typical PL spectra of ZnO nanocombs and nanorods. (*b*) The energy-dispersed spectroscopy (EDS) of ZnO nanocombs, and the inset shows the element ratio of Zn : O.

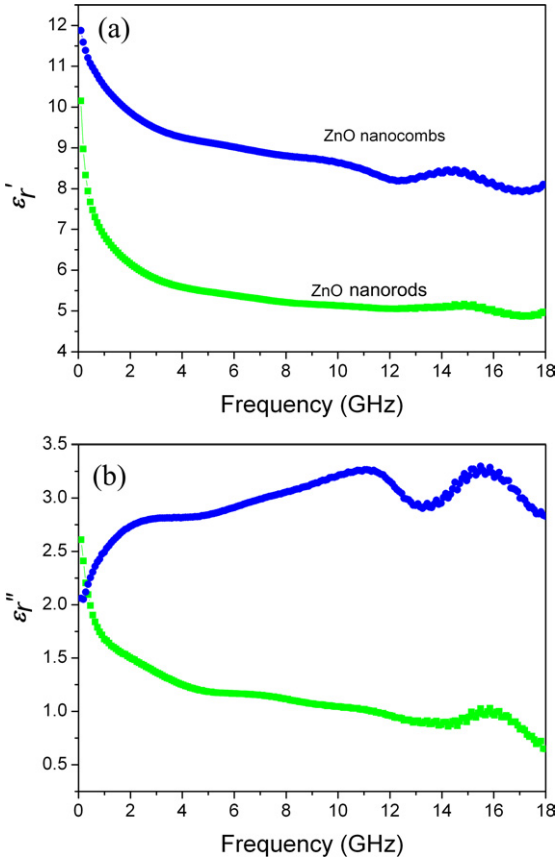

Figure 13. (*a*) The real permittivity of the ZnO nanorod composite with 50% ZnO nanorods and the ZnO nanocomb composite with 50 vol% ZnO nanocombs. (*b*) The imaginary permittivity of the two ZnO composites.

values decline with increasing frequency from 2.5 to 0.5 in 0.1–18 GHz and exhibit a peak at 13–17 GHz. However, for the ZnO nanocombs composite, the ε_r'' values increase from 1 to 2 and the curve exhibits two peaks at 11 GHz and 16 GHz. The imaginary part ε_r'' of ZnO nanocombs is relatively higher in contrast to ZnO nanowires, which implies the distinct dielectric loss properties arising from the morphology variation. The reflection loss (RL) curves are calculated according to the following equations [39]:

$$Z_{in} = Z_0(\mu_r\varepsilon_r)^{1/2}\tanh[j(2\pi fd/c)(\mu_r\varepsilon_r)^{1/2}], \quad (1)$$

$$\mathrm{RL(dB)} = 20\log|(Z_{in} - Z_0)/(Z_{in} + Z_0)|, \quad (2)$$

where f is the frequency of the EM wave, d the thickness of the absorber, c the velocity of light, Z_0 the impedance of free space and Z_{in} the input impedance of the absorber. According to equations (1) and (2), the simulations of the RL of the two ZnO composites with a thickness of 3.0 mm are shown in figure 14(*a*). The ZnO nanocomb composite possesses stronger microwave absorption property than the nanowire composite. Figure 14(*b*) shows simulations of the RL of the ZnO nanocomb composite with different thicknesses. The value of the minimum RL is −12 dB at 11 GHz for the ZnO nanocomb composite with a thickness of 2.5 mm. Our results are similar to that given in the literature [6].

According to the results shown above, ZnO nanocombs have strong absorption of microwaves. It can be noted that the ZnO nanocombs have a unique hierarchical morphology. Such a structure may form some discontinuous networks in the composite. It is easy for the electromagnetic wave to penetrate the porous layer formed by the numerous conductive networks of comb-like ZnO and the energy is induced into dissipative current, which leads to energy attenuation [6]. More importantly, due to the large aspect ratio and the dielectric confinement effect of the ZnO nanocombs, the charge concentration at the tips of the branches is distinct when the material is under an electric field. Thus, it is reasonable that the concentrated tips of the branches will act as multipoles that will be tuned with the incident microwaves and contribute to strong absorption. The interfacial electric polarization should also be considered. The multi-interfaces between branches, paraffin matrix and air bubbles can be of benefit for microwave absorption because of the interaction of electromagnetic radiation with charge multipoles at the interfaces [6]. However, further experimental and theoretical investigation is needed to make the mechanism clear.

4. Conclusion

In summary, ZnO nanocombs and nanorods with different morphologies have been successfully synthesized through a simple MVD route at 600–750 °C using pure zinc powder or zinc and graphite powders as source materials. Further experiments show that the morphology of the final product in the thermal-evaporation process is mainly influenced by

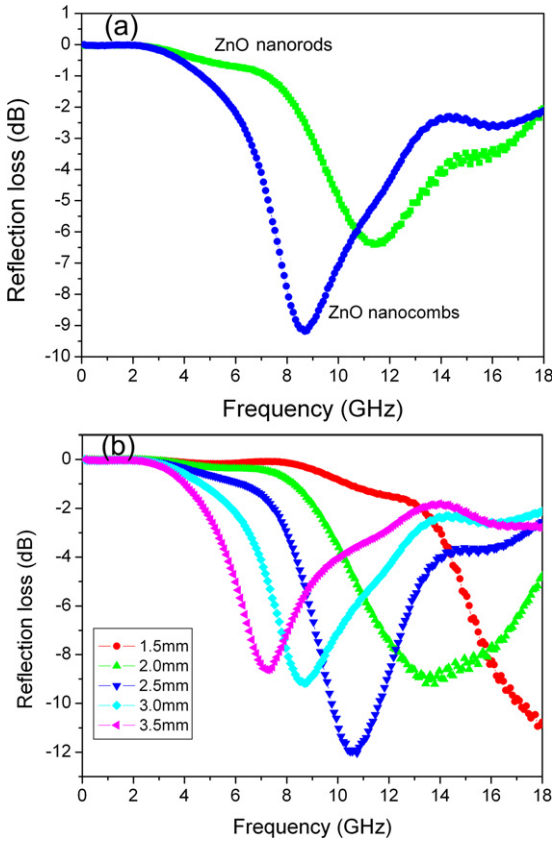

Figure 14. (*a*) The simulations of the RL for the two ZnO composites with a thickness of 3.0 mm. (*b*) The simulations of the RL of the ZnO nanocomb composite with different thicknesses.

the following four factors: reaction temperature, the distance between the source and the substrates, the kind of substrates and the kind of precursors. Our results support that the Zn-terminated (0 0 0 1) surface is chemically active for inspiring self-catalysis, which leads to the formation of the comb structure. PL properties show that there are sharp UV emissions and broad defect-related green emissions for all products. The relative intensity of the UV emission to defect-related green emissions decreases from ZnO nanorods to nanocombs. Microwave absorption properties of these nanocombs are also investigated. The value of the minimum RL is −12 dB at 11 GHz for the ZnO nanocomb composite with a thickness of 2.5 mm. Such strong absorption is attributed to the unique branched morphology of the ZnO nanocombs in the composite. Our results suggest that nanostructures of this type are ideal objects for the fabrication of nanoscale functional devices and may find applications in a variety of fields.

Acknowledgments

This work was supported by the fund from the National Natural Science Foundation of China (Grant No 60376039).

References

[1] Xia Y N, Yang P D, Sun Y G, Wu Y Y, Mayers B, Gates B, Yin Y D, Kim F and Yan H Q 2003 *Adv. Mater.* **15** 353–89
[2] Pan Z W, Dai Z R and Wang Z L 2001 *Science* **291** 1947–9
Wang Z L and Song J H 2006 *Science* **312** 242–6
Wang X D, Song J H and Wang Z L 2007 *Science* **316** 102–5
Wang Z L 2007 *Adv. Mater.* **19** 889–92
Qin Y, Wang X D and Wang Z L 2008 *Nature* **451** 809–13
[3] Comini E, Faglia G, Sberveglieri G, Pan Z W and Wang Z L 2002 *Appl. Phys. Lett.* **81** 1869–71
[4] Bai X D, Gao P X, Wang Z L and Wang E G 2003 *Appl. Phys. Lett.* **82** 4806–8
[5] Zhou J, Xu N S and Wang Z L 2006 *Adv. Mater.* **18** 2432–5
[6] Chen Y J, Cao M S, Wang T H and Wan Q 2004 *Appl. Phys. Lett.* **84** 3367–9
Tang X and Hu K A 2007 *Mater. Sci. Eng.* B **139** 119–23
Cao M S, Shi X L, Fang X Y, Jin H B, Hou Z L and Zhou W 2007 *Appl. Phys. Lett.* **91** 203110
[7] Huang M H, Mao S, Feick H, Yan H, Wu Y, Kind H, Weber E, Russo R and Yang P D 2001 *Science* **292** 1897
[8] Gao P X and Wang Z L 2002 *J. Phys. Chem.* B **106** 12653
Gao P X, Ding Y and Wang Z L 2003 *Nano Lett.* **3** 1315
Gao P X and Wang Z L 2004 *Appl. Phys. Lett.* **84** 2883
[9] Sounart T L, Liu J, Voigt J A, Spoerke E D and McKenzie B 2007 *J. Am. Chem. Soc.* **129** 15786
Sounart T L, Liu J, Voigt J A, Hsu J W P, Spoerke E D, Tian Z and Jiang Y B 2006 *Adv. Funct. Mater.* **16** 335
Jiang P, Zhou J J, Fang H F, Wang C Y, Wang Z L and Xie S S 2007 *Adv. Funct. Mater.* **17** 1303
May S J, Zheng J G, Wessels B W and Lauhou L J 2005 *Adv. Mater.* **17** 598
Li P, Liu H, Zhang Y F, Wei Y and Wang X K 2007 *Mater. Chem. Phys.* **106** 63
[10] Lao J Y, Wen J G and Ren Z F 2002 *Nano Lett.* **2** 1287
Lao J Y, Huang J Y, Wang D Z and Ren Z F 2004 *J. Mater. Chem.* **14** 770
Banerjee D, Lao J Y, Wang D Z, Huang J Y and Ren Z F 2003 *Appl. Phys. Lett.* **83** 2061
[11] Zhang J, Yang Y D, Jiang F H, Xu B L and Li J P 2005 *J. Solid State Chem.* **178** 2804
Zhao F H, Li X Y, Zheng J G, Yang X F, Zhao F L, Wong K S, Wang J, Lin W J, Wu M M and Su Q 2008 *Chem. Mater.* **20** 1197
[12] Wang Z L 2004 *Mater. Today* **7** 26
Wang Z L 2007 *MRS Bull.* **32** 109
[13] Wang Z L, Kong X Y and Zuo J M 2003 *Phys. Rev. Lett.* **91** 185502
[14] Gao P X and Wang Z L 2003 *J. Am. Chem. Soc.* **125** 11299
[15] Kong X Y, Ding Y, Yang R and Wang Z L 2004 *Science* **303** 1348
[16] Kong X Y and Wang Z L 2003 *Nano Lett.* **3** 1625
Gao P X, Ding Y, Mai W, Hughes W L, Lao C S and Wang Z L 2005 *Science* **309** 1700
[17] Hughes W L and Wang Z L 2004 *J. Am. Chem. Soc.* **126** 6703
[18] Li F, Ding Y, Gao P X, Xin X and Wang Z L 2004 *Angew. Chem.* **116** 5350
Gao P X, Lao C S, Ding Y and Wang Z L 2006 *Adv. Funct. Mater.* **16** 53
[19] Quan H Q, He R R, Pham J and Yang P D 2003 *Adv. Mater.* **15** 402
[20] Lyu S C, Zhang Y, Lee C J, Ruh H and Lee H J 2003 *Chem. Mater.* **15** 3294
Park J H, Choi H J, Choi Y J, Sohn S H and Park J G 2004 *J. Mater. Chem.* **14** 35
Leung Y H, Djurisic A B, Gao J, Xie M H, Wei Z F, Xu S J and Chan W K 2004 *Chem. Phys. Lett.* **394** 452
Shen G Z, Bando Y S and Lee C J 2005 *J. Phys. Chem.* B **109** 10779
[21] Yan H Q, He R R, Johnson J, Law M, Saykally R J and Yang P D 2003 *J. Am. Chem. Soc.* **125** 4728
[22] Wang J X, Sun X W, Wei A, Lei Y, Cai X P and Li C M 2006 *Appl. Phys. Lett.* **88** 233106

[23] Pan Z W, Mahurin S M, Dai S and Lowndes D H 2005 *Nano Lett.* **5** 723
[24] Huang H B, Yang S G, Gong J F, Liu H W, Duan J H, Zhao X N, Zhang R, Liu Y L and Liu Y C 2005 *J. Phys. Chem.* B **109** 20746
Chen Y Q, Jiang J, He Z Y, Su Y, Cai D and Chen L 2005 *Mater. Lett.* **59** 3280
Xu C X, Sun X W, Dong Z L and Yu M B 2004 *J. Cryst. Growth* **270** 498
[25] Lao C S, Gao P X, Yang R S, Zhang Y, Dai Y and Wang Z L 2005 *Chem. Phys. Lett.* **417** 359
[26] Li C, Fang G J, Su F H, Li G H, Wu X G and Zhao X Z 2006 *Cryst. Growth. Des.* **6** 2588
[27] Liu J Z, Yan P X, Yue G H, Chang J B, Zhuo R F and Qu D M 2006 *Mater. Lett.* **60** 3122
[28] Qiao L, Wen F S, Wei J Q, Wang J B and Li F S 2008 *J. Appl. Phys.* **103** 063903
[29] Bundesmann C, Ashkenov N, Schubert M, Spemann D, Butz T, Kaidashev E M, Lorenz M and Grundmann M 2003 *Appl. Phys. Lett.* **83** 1974
[30] Du C L, Gu Z B, Lu M H, Wang J, Zhang S T, Zhao J, Cheng G X, Heng H and Chen Y F 2006 *J. Appl. Phys.* **99** 123515
[31] Calleja J M and Cardona M 1977 *Phys. Rev.* B **16** 3753
Scott J F 1970 *Phys. Rev.* B **2** 1209
Ng H T, Chen B, Li J, Han J, Meyyappan M, Wu J, Li S X and Haller E E 2003 *Appl. Phys. Lett.* **82** 2023
Du C L, Gu Z B, You Y M, Kasim J, Yu T, Shen Z X, Ni Z H, Ma Y, Cheng G X and Chen Y F 2008 *J. Appl. Phys.* **103** 023521
[32] Shen G Z, Bando Y S, Liu B D, Golberg D and Lee C J 2006 *Adv. Funct. Mater.* **16** 410
Shen G Z, Cho J H and Lee C J 2005 *Chem. Phys. Lett.* **401** 414
[33] Wang M J and Wada D H 1990 *J. Mater. Sci.* **25** 1690
Jiang G J, Zhuang H R, Zhang J, Ruan M L, Li W L, Wu F Y and Zhang B L 2000 *J. Mater. Sci.* **35** 63
Seo W and Koumoto K 1996 *J. Am. Ceram. Soc.* **79** 1777
[34] Sears G W 1956 *Acta Metall.* **3** 268
Zhang Y J, Wang N L, Gao S P, He R R, Miao S, Liu J, Zhu J and Zhang X 2002 *Chem. Mater.* **14** 3564
[35] Moore D, Ronning C, Ma C and Wang Z L 2004 *Chem. Phys. Lett.* **385** 8
Moore D, Ding Y and Wang Z L 2006 *Angew. Chem. Int. Edn* **45** 5150
[36] Lautenschlaeger S, Sann J, Volbers N and Meyer B K 2008 *Phys. Rev.* B **77** 144108
[37] Banerjee D, Lao J Y, Wang D Z, Huang J Y, Steeves D, Kimball B and Ren Z F 2004 *Nanotechnology* **15** 404
Pan A L, Liu R B, Wang S Q, Wu Z Y, Cao L, Xie S S and Zou B S 2005 *J. Cryst. Growth* **282** 125
Huang M H, Wu Y Y, Feick N T, Weber E and Yang P D 2001 *Adv. Mater.* **13** 113
Lin B, Fu Z and Jia Y 2001 *Appl. Phys. Lett.* **79** 943
[38] Studenikin S A and Cocivera M 2002 *J. Appl. Phys.* **91** 5060
Reynolds D C, Look D C and Jogai B 2001 *J. Appl. Phys.* **89** 6189
Özgür Ü, Alivov Y I, Liu C and Teke A 2005 *J. Appl. Phys.* **98** 041301
[39] Matsumoto M and Miyata Y 1997 *IEEE Trans. Magn.* **33** 4459